Supplementary Information for

Graphdiyne supported metal alloy on atom level for the efficient cycloaddition reaction of CO_2

Zhiqiang Zheng[a], Yiyang Zheng[a], Lu Qi [a], Xue Yurui*[a], Yuliang Li *[abc]

[a]Shandong Provincial Key Laboratory for Science of Material Creation and Energy Conversion, Science Center for Material Creation and Energy Conversion, School of Chemistry and Chemical Engineering, Shandong University, Jinan 250100, China.

[b]CAS Key Laboratory of Organic Solids, Institute of Chemistry, Chinese Academy of Sciences, Beijing 100190, China.

[c]University of Chinese Academy of Sciences, Beijing 100049, P.R. China.

E-mail: ylli@iccas.ac.cn (Y. Li)

1. Experimental sections

1.1 Materials

All of the chemicals were of analytical grade in this study, and used without further purification. The hexakis[(trimethylsilyl)ethynyl]benzene, tetrabutylammonium fluoride (TBAF, 1.0 M in THF), $IrCl_3$, CuCl, NaBr, KI and styrene oxide were purchased from Energy Chemical unless special description. The hexakis[(trimethylsilyl)ethynyl]benzene was used after deprotection of functional groups throuth TBAF immediately.

1.2 Synthesis of IrCu-Cl/GDY dual atom catalyst

A mixture of 66.6 mg (0.3 mmol) hexaethynylbenzene, 36 mg (0.1 mmol) $IrCl_3 \cdot 3H_2O$ and 10 mg (0.1 mmol) CuCl were added in 40 mL dry pyridine, stirred for 60 min, then the solution was heated to 60 ℃ and maintained for 3 days under the dark condition. The obtained precipitate was collected by vacuum filtration and washed by N, N-Dimethylformamide (DMF), water and ethanol for three times, finally dried under the vacuum at an ambient condition for 12h.

1.3 Ligand exchange procedure of IrCu-Cl/GDY

100 mg IrCu-Cl/GDY was suspended in the saturated NaBr or KI solution, the mixture was heated to 60 ℃ and stirred for 12 h. The obtained precipitate was collected by vacuum filtration and washed by water and ethanol for three times, finally dried under the vacuum at an ambient condition for 12h.

1.4 Characterizations

The morphology of the catalyst was characterized by scanning electron microscope (SEM), Apreo, Thermo Scientific), high-resolution transmission electron microscope (HRTEM), Talos F200XG2 TEM, Thermo Scientific, and high angle annular dark field scanning transmission electron microscopy (HAADF), JEM-ARM200F, JEOL. Energy-dispersive X-ray spectroscopy (EDX) was collected with an energy-dispersive X-ray detector in JEM-ARM200F and Talos F200X G2 TEM. The metal content in

PtCu/GDY was determined by inductively coupled plasma optical emission spectrometry (ICP-OES), NexION 1000G, PerkinElmer. Raman spectra were collected by LabRAM HR800 spectrometer through a 473 nm excitation laser source. XPS measurements were recorded through the Thermo Scientific Nexsa instrument with monochromatic Al Kα X-ray radiation. In situ diffuse reflectance infrared Fourier transform spectroscopy (DRIFTS) was taken in VERTEX 70v, Bruker. The yield and purity of the products was determined by nuclear magnetic resonance spectroscopy (^{1}H NMR), AVANCE III HD 400, Bruker.

1.5 Cycloaddition reactions

In a typical procedure, IrCu/GDY (40 mg) and styrene oxide (2 ml) were added into a teflon-lined stainless-steel autoclave under 100 ℃ and 1 MPa for different reaction times. The variable temperature experiment was conducted for 12 h at set temperature. The resulted mixture was directly analyzed by ^{1}H NMR for the purity and yield of final products.

1.6 In situ DRIFTS measurements

The in situ diffuse reflectance infrared Fourier transform spectroscopy (DRIFTS) were obtained on Bruker VERTEX 70v spectrophotometer with a wavenumber resolution of 4 cm^{-1} by scanning 32 times. 10 mg catalyst mixed with 50 μL styrene oxide was placed in the sample chamber, sealed with a dome. The chamber was heated to 100 ℃ and the background spectrum was obtained, then the CO_2 stream (10 mL/min) was allowed to flow into the sample chamber. In situ spectrum was collected at 60 s intervals during the CO_2 cycloaddition experiment.

1.7 XAS measurements and analysis

The X-ay absorption spectra were collected at 1W1B station in in Beijing Synchrotron Radiation Facility (BSRF). The storage rings of BSRF were operated at 2.5 GeV, and the average current was 250 mA. Si(111) double crystal monochromator was used, the data collection were carried out in transmission mode using ionization chamber. All of

the spectra were recorded in the ambient conditions. The acquired data were processed through the standard procedures by using the ATHENA module implemented in the IFEFFIT software packages.

2. Computational details

All of the calculations are performed in the framework of the spin-polarized density functional theory with the projector augmented plane-wave method, as implemented in the Vienna ab initio simulation package (VASP)[1,2]. The generalized gradient approximation (GGA) proposed by Perdew, Burke, and Ernzerhof (PBE) is selected for the exchange-correlation potential[3,4]. The long-range van der Waals interaction is described by the DFT-D3 approach[5]. The cut-off energy for plane wave is set to 480 eV. The energy criterion is set to 10^{-5} eV in iterative solution of the Kohn-Sham equation. All the structures are relaxed until the residual forces on the atoms have declined to less than 0.02 eV/Å. Data analysis and visualization are carried out with the help of VASPKIT[6] code and VESTA[7]. To avoid interlaminar interactions, a vacuum spacing of 20 Å is applied perpendicular to the slab. Here, we define $\Delta\rho=\rho_{A+B}-\rho_A-\rho_B$ as the charge density difference of A/B heterostructure, where $\rho_{A/B}$, ρ_A and ρ_B are the charge densities of A/B heterostructure, isolated A and B slabs, respectively.

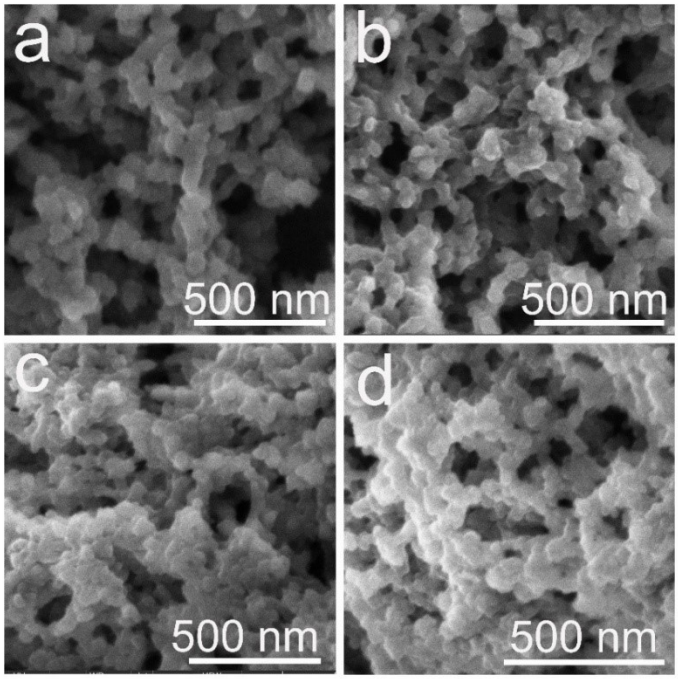

Fig. S1. SEM images of IrCu-Cl/GDY.

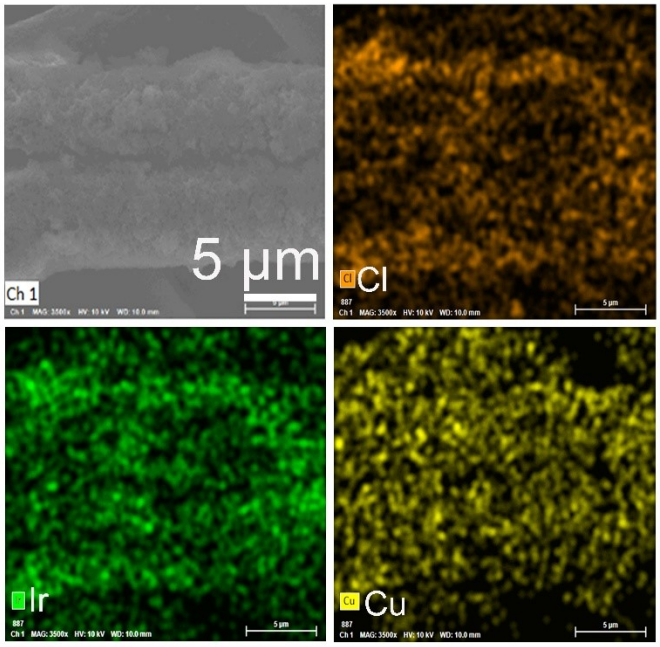

Fig. S2. Element mapping images of Cl, Ir and Cu in IrCu-Cl/GDY from SEM equipped with EDX.

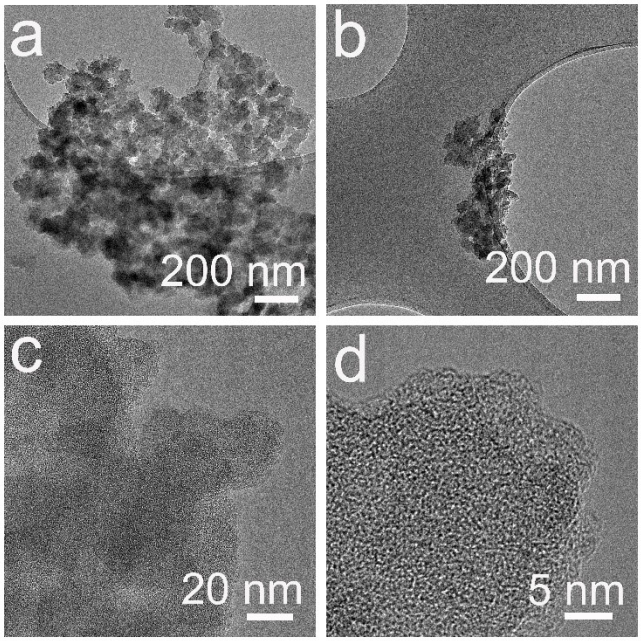

Fig. S3. TEM and HRTEM images of IrCu-Cl/GDY.

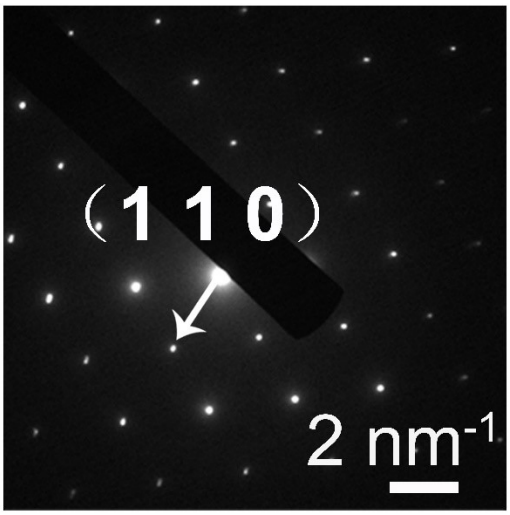

Fig. S4. SAED image of IrCu-Cl/GDY.

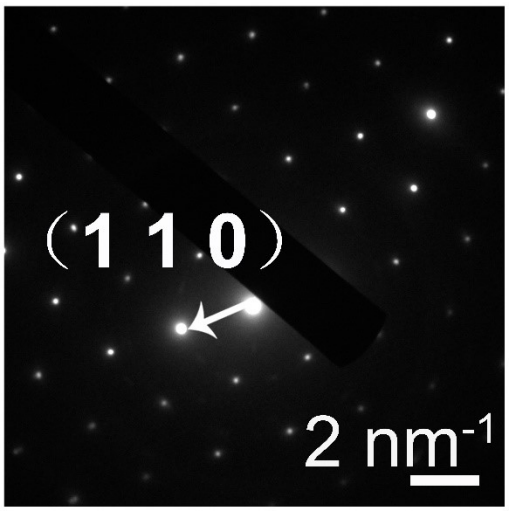

Fig. S5. SAED image of GDY.

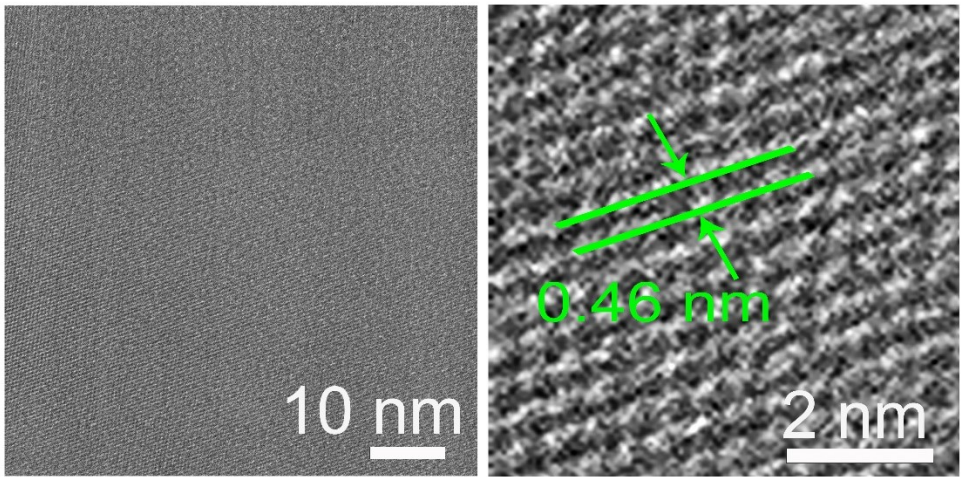

Fig. S6. HRTEM images of GDY.

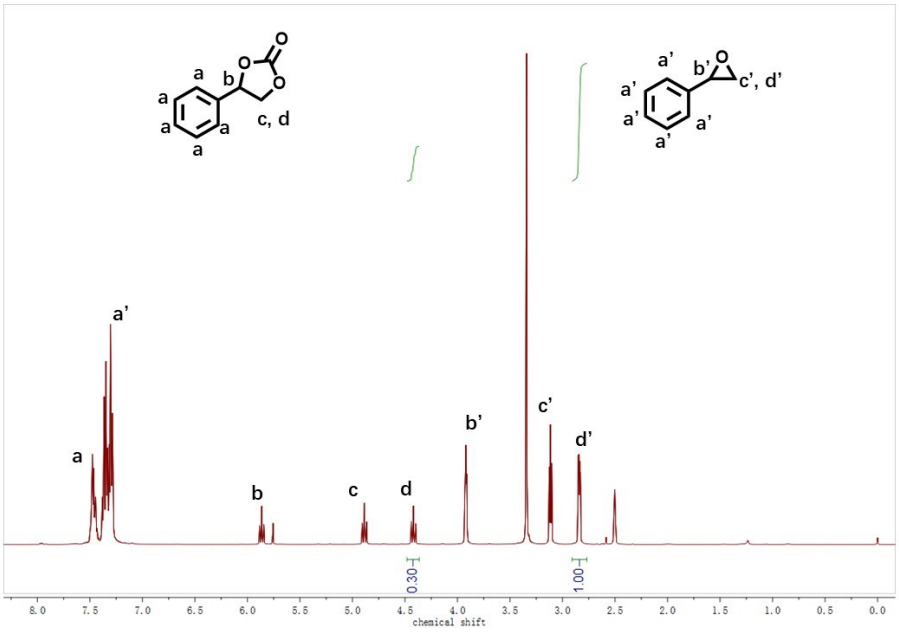

Fig. S7. ^{1}H NMR (400 MHz, DMSO-d6) spectrum of reaction mixture performed at 100 ℃ for 12 h with IrCu-Cl/GDY.

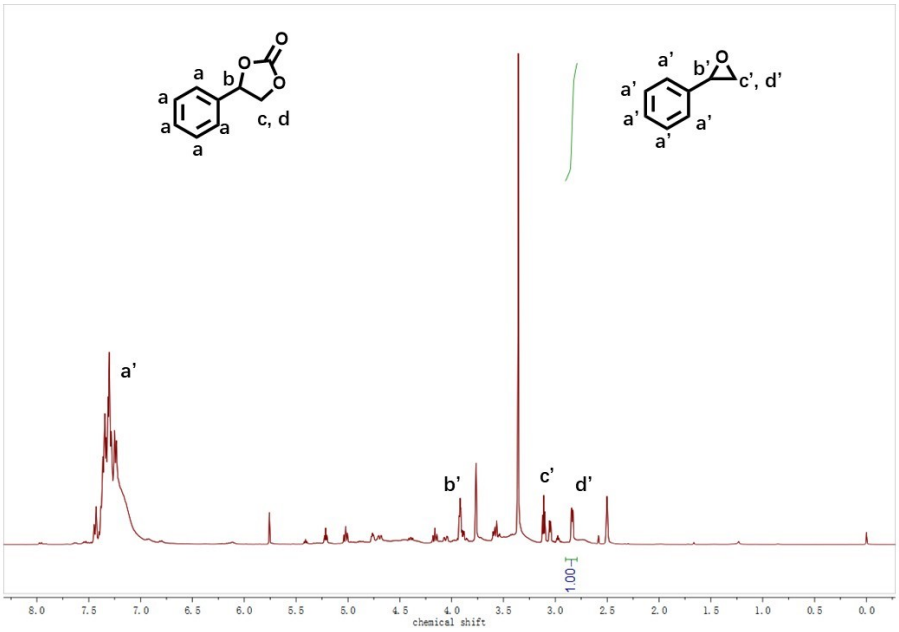

Fig. S8. ^{1}H NMR (400 MHz, DMSO-d_6) spectrum of reaction mixture performed at 100 °C for 12 h with $IrCl_3$.

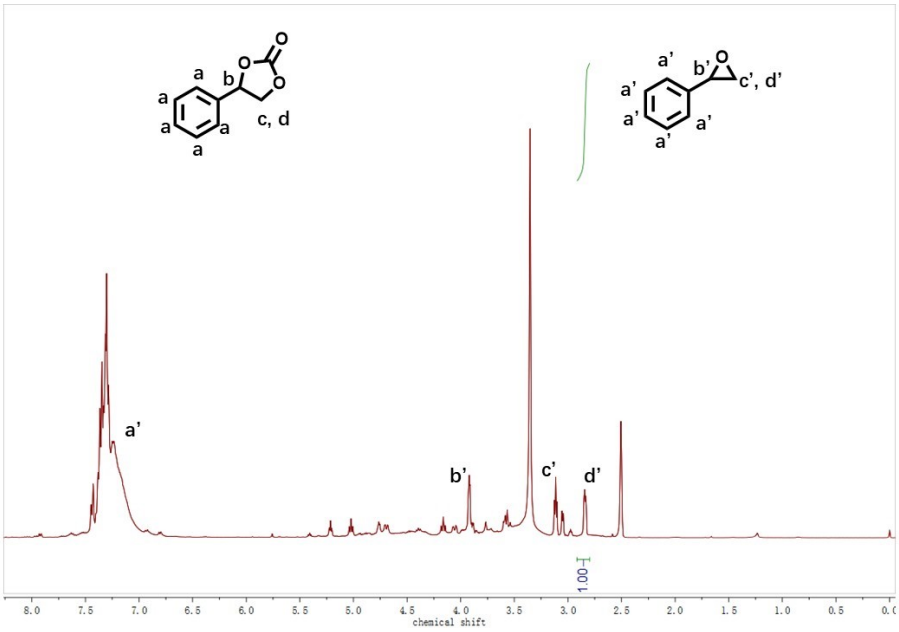

Fig. S9. ^{1}H NMR (400 MHz, DMSO-d6) spectrum of reaction mixture performed at 100 ℃ for 12 h with CuCl.

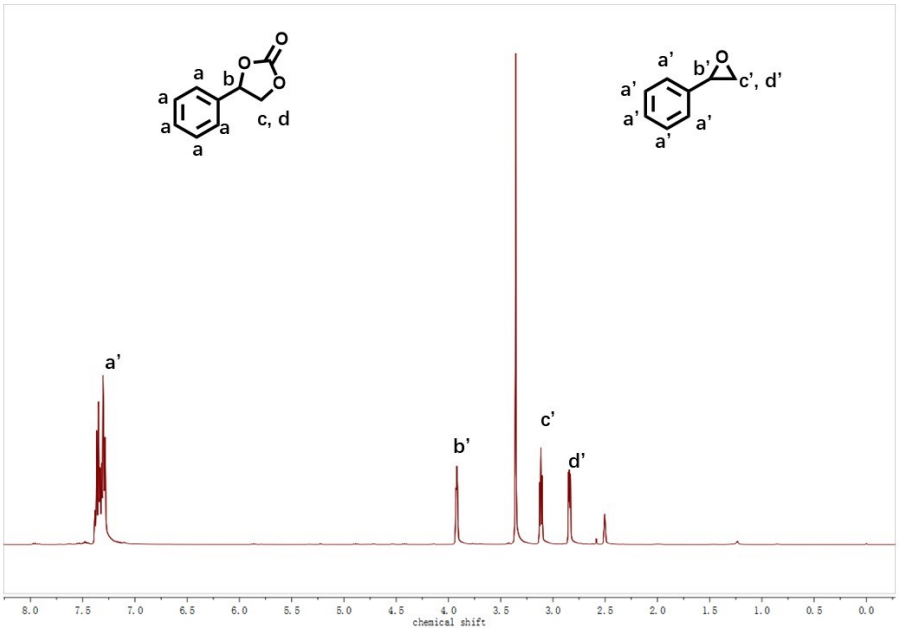

Fig. S10. ^{1}H NMR (400 MHz, DMSO-d6) spectrum of reaction mixture performed at 100 ℃ for 12 h with GDY.

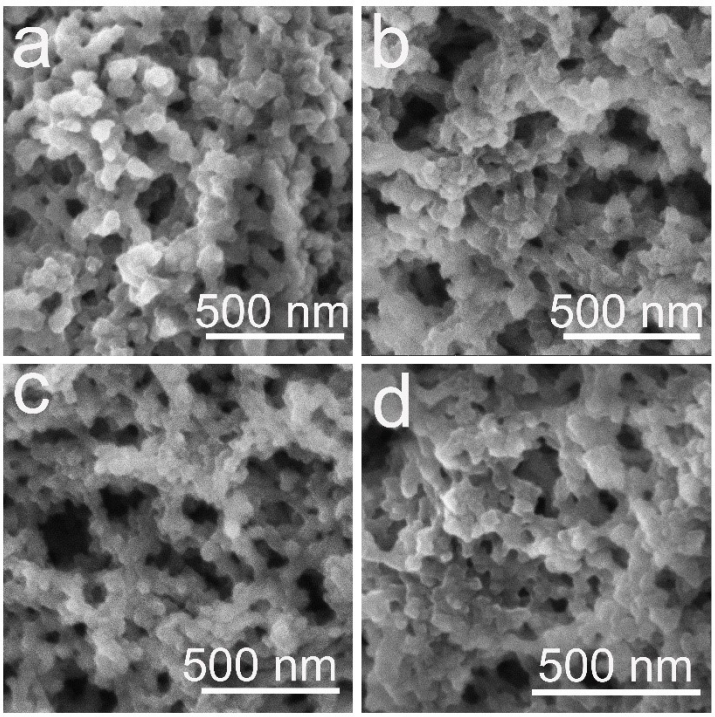

Fig. S11. SEM images of IrCu-I/GDY.

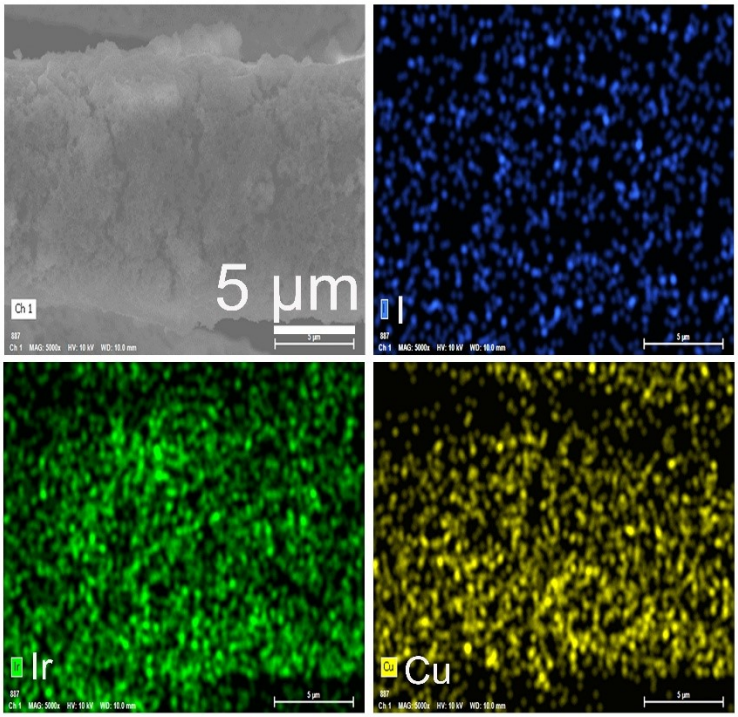

Fig. S12. Element mapping images of I, Ir and Cu in IrCu-I/GDY from SEM equipped with EDX.

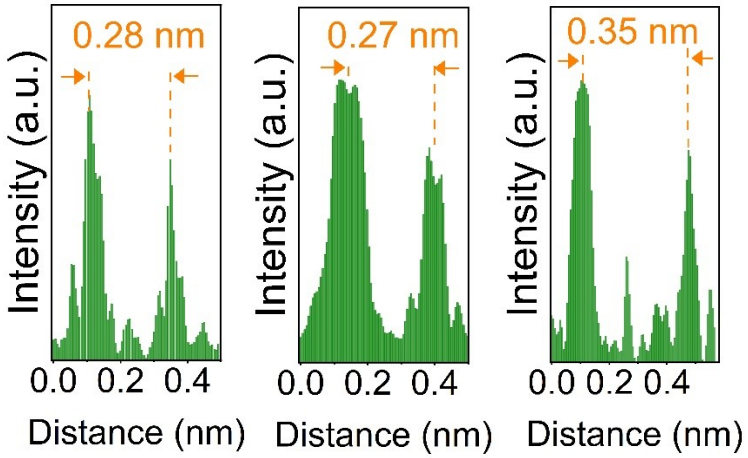

Fig. S13. Line scan intensity profile derived from three areas in IrCu-I/GDY.

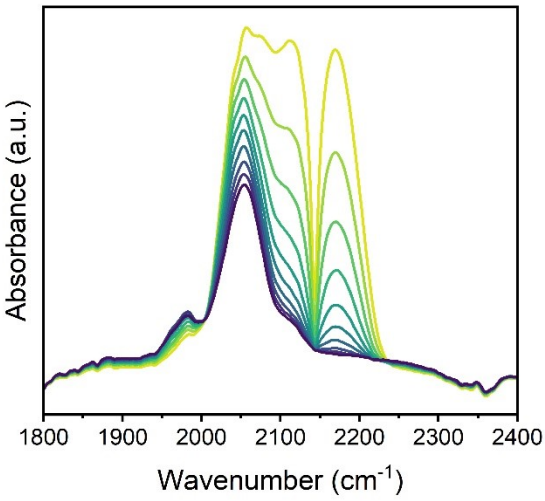

Fig. S14. In situ CO-DRIFTS spectra of the IrCu-Br/GDY.

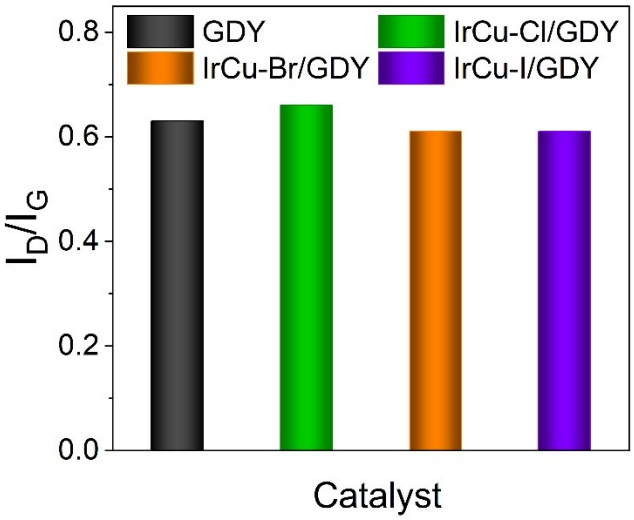

Fig. S15. ID/IG ratio of GDY and IrCu/GDY calculated from Raman spectrum.

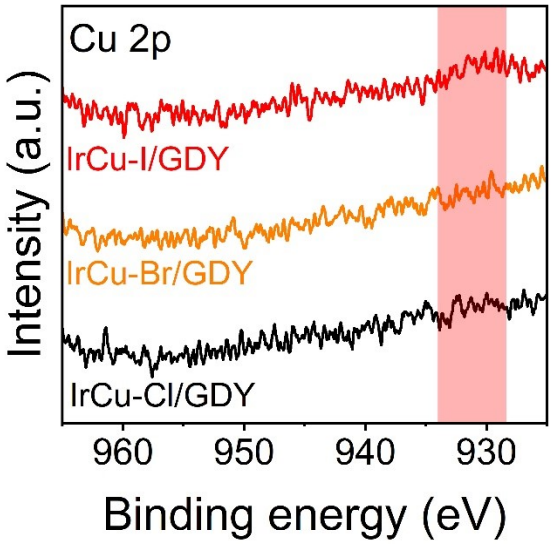

Fig. S16. Cu 2p XPS spectra of IrCu-Cl/GDY, IrCu-Br/GDY and IrCu-I/GDY.

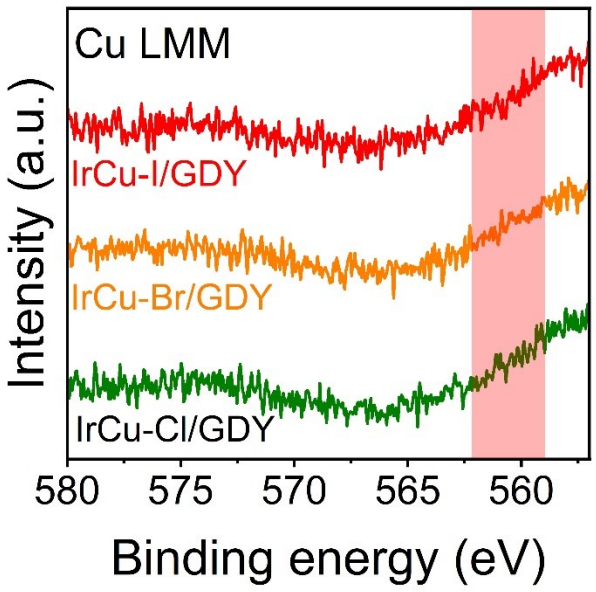

Fig. S17. Cu LMM Auger spectrum of IrCu-Cl/GDY, IrCu-Br/GDY and IrCu-I/GDY.

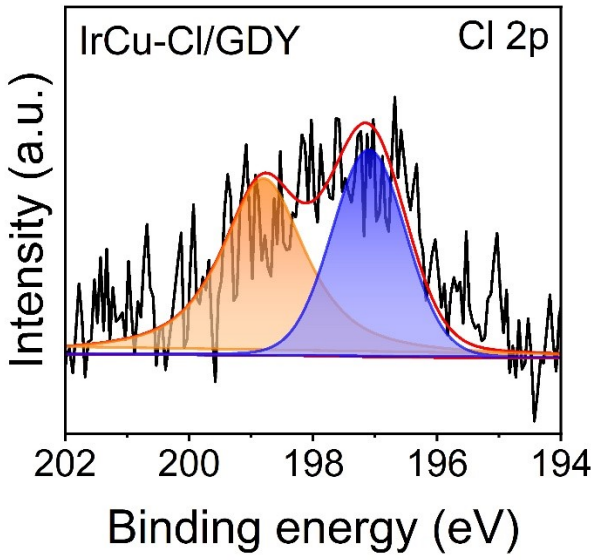

Fig. S18. Cl 2p XPS spectrum of IrCu-Cl/GDY.

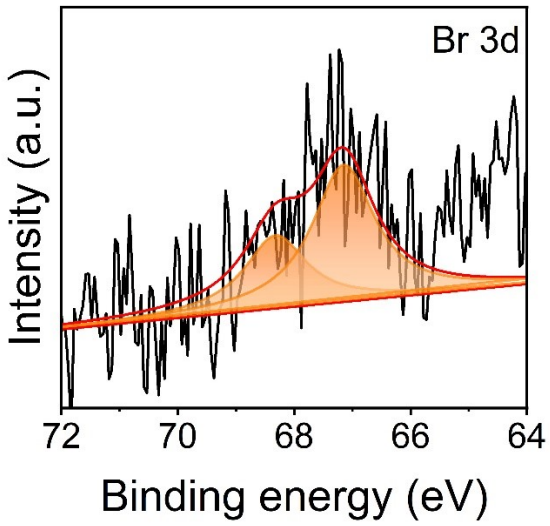

Fig. S19. Br 3d XPS spectrum of IrCu-Br/GDY.

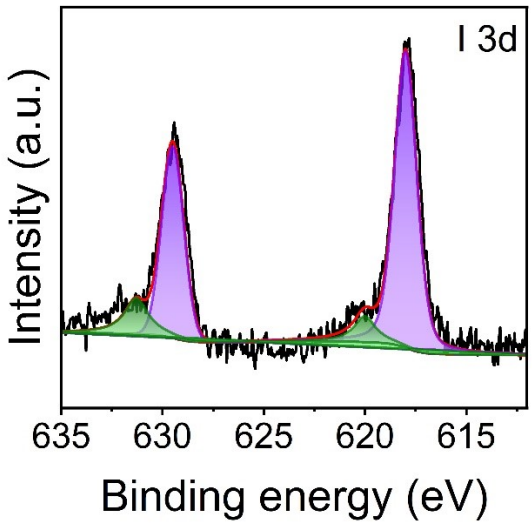

Fig. S20. I 3d XPS spectrum of IrCu-I/GDY.

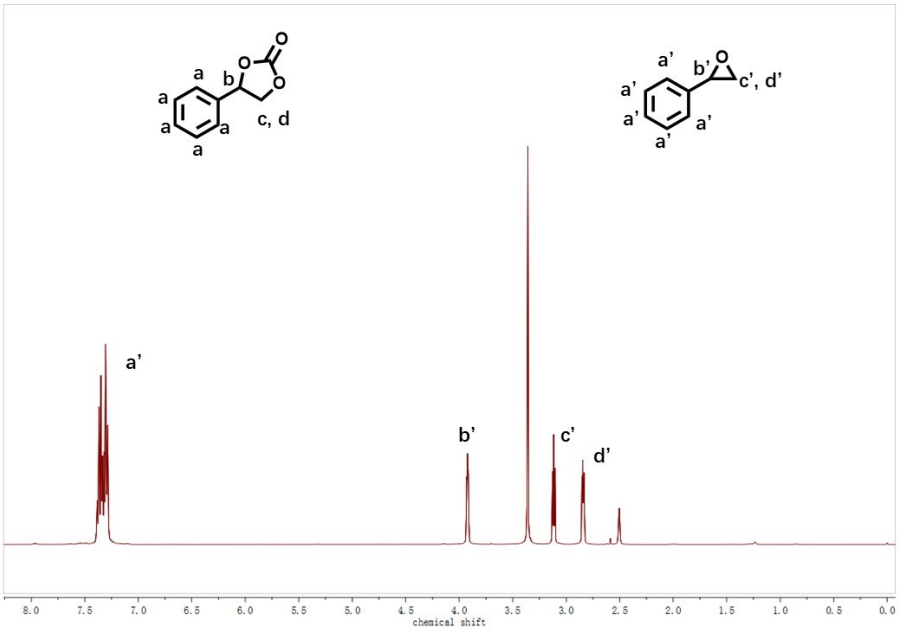

Fig. S21. ^{1}H NMR (400 MHz, DMSO-d6) spectrum of reaction mixture performed at 100 ℃ for 12 h with NaCl.

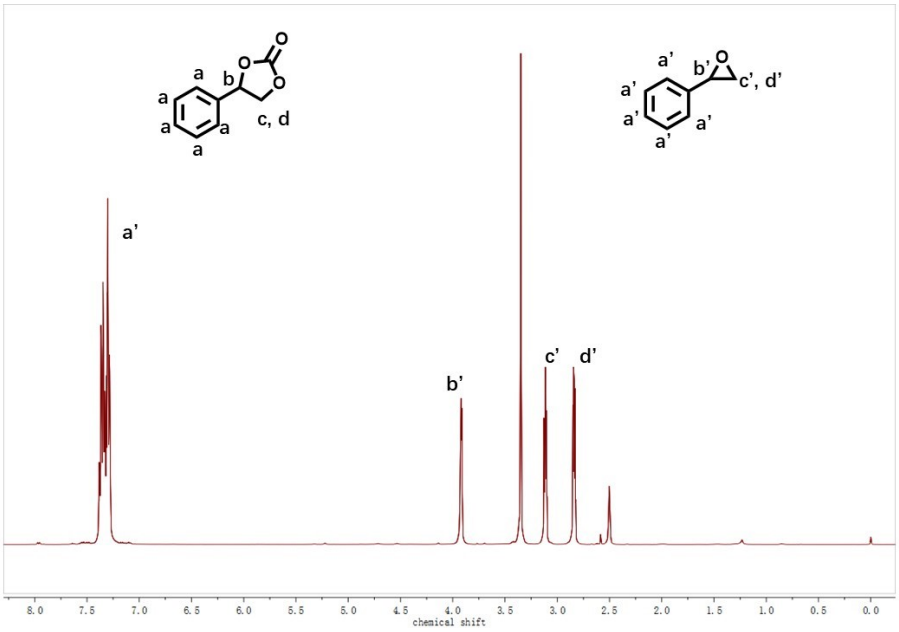

Fig. S22. ^{1}H NMR (400 MHz, DMSO-d6) spectrum of reaction mixture performed at 100 ℃ for 12 h with NaBr.

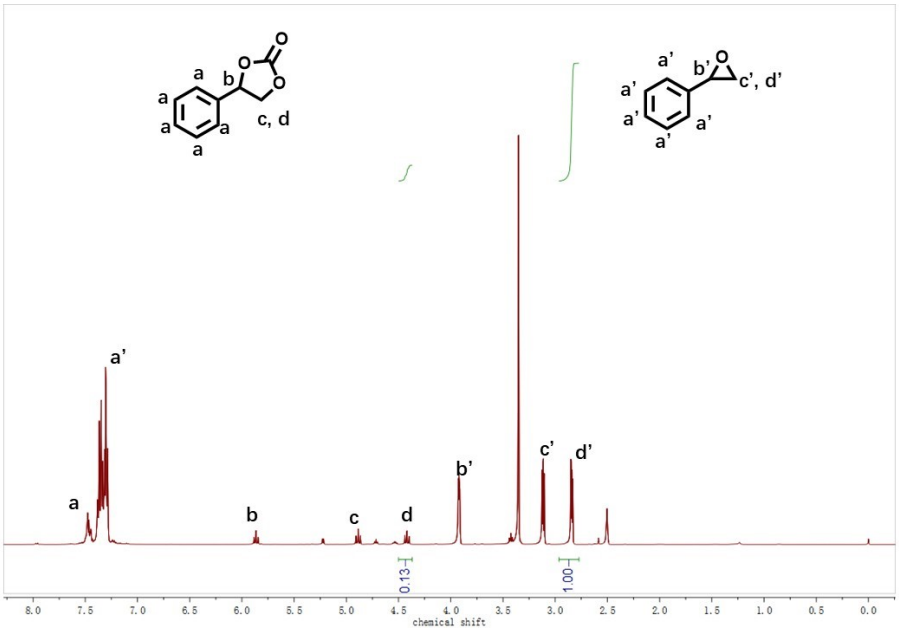

Fig. S23. ^{1}H NMR (400 MHz, DMSO-d6) spectrum of reaction mixture performed at 100 ℃ for 12 h with KI.

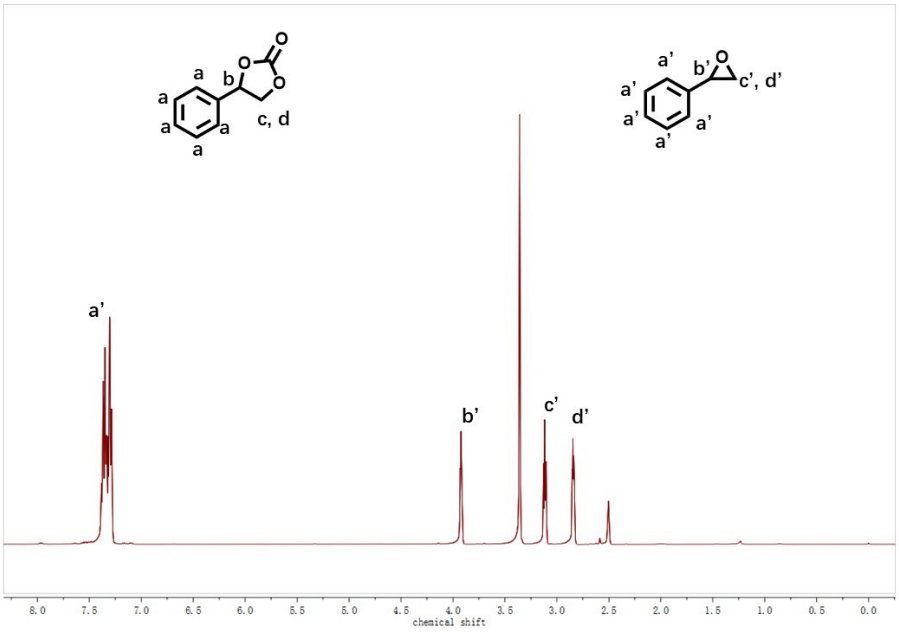

Fig. S24. ^{1}H NMR (400 MHz, DMSO-d6) spectrum of reaction mixture performed at 100 ℃ for 12 h with GDY-Cl.

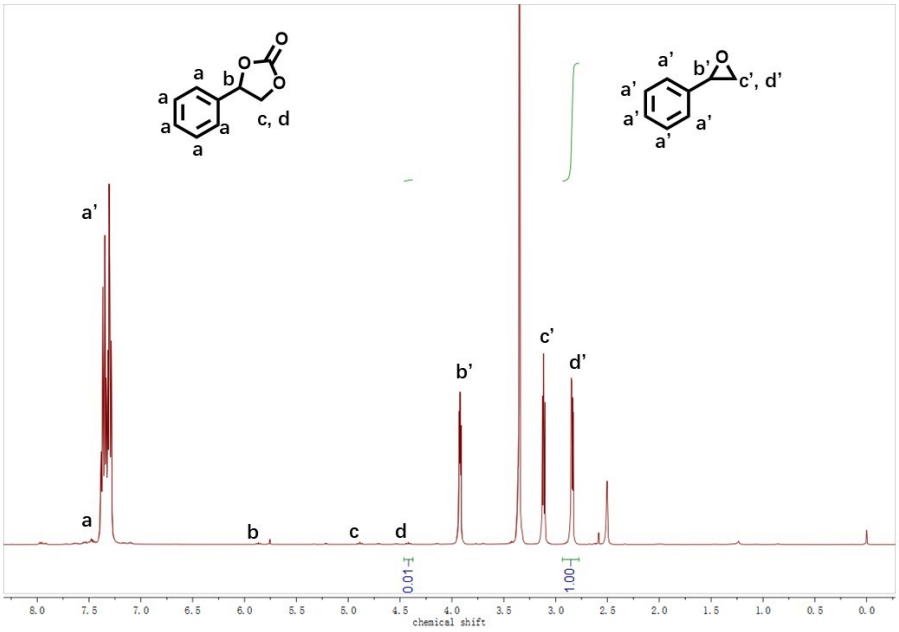

Fig. S25. ^{1}H NMR (400 MHz, DMSO-d6) spectrum of reaction mixture performed at 100 ℃ for 12 h with GDY-Br.

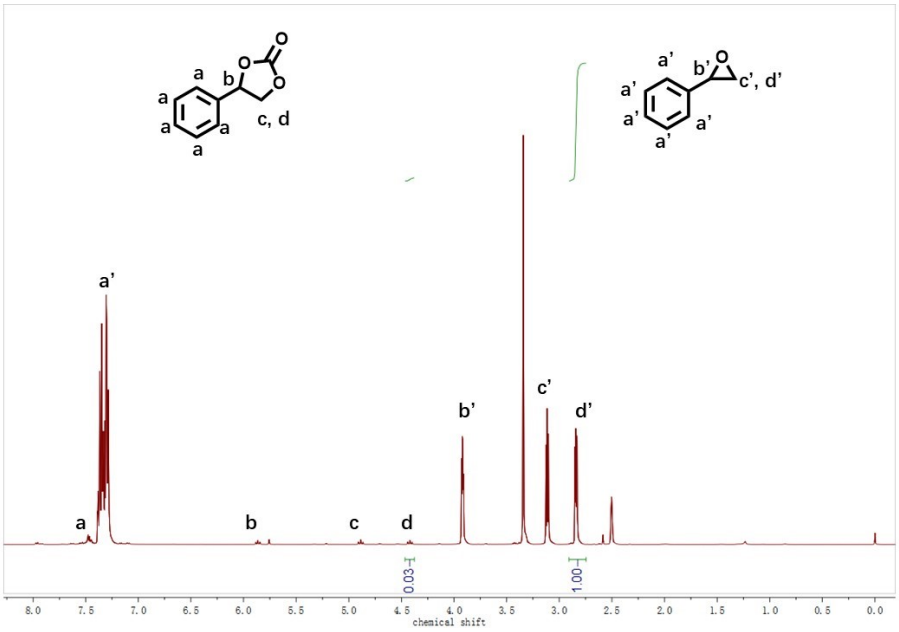

Fig. S26. ^{1}H NMR (400 MHz, DMSO-d6) spectrum of reaction mixture performed at 100 ℃ for 12 h with GDY-I.

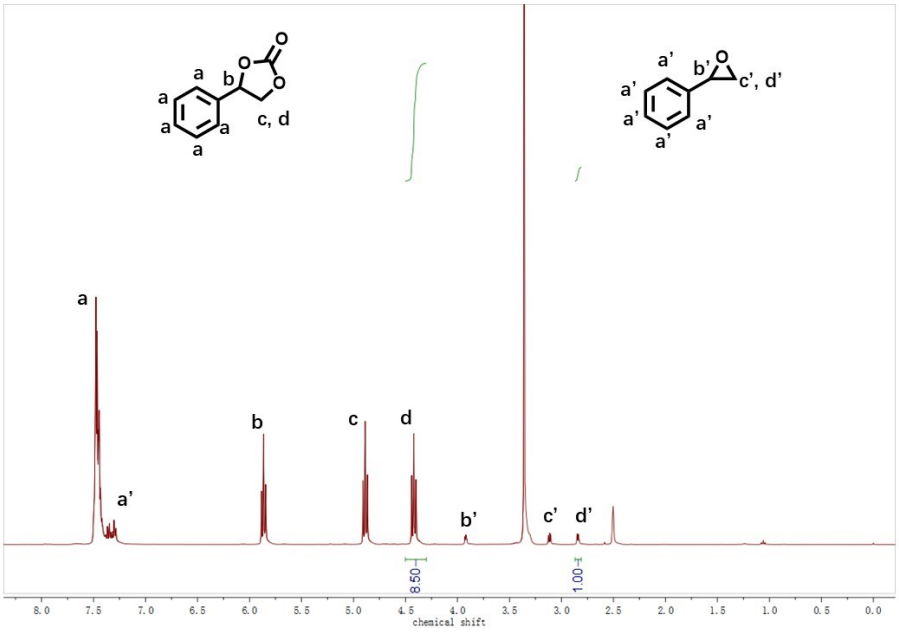

Fig. S27. ^{1}H NMR (400 MHz, DMSO-d6) spectrum of reaction mixture performed at 100 °C for 12 h with IrCu-Br/GDY.

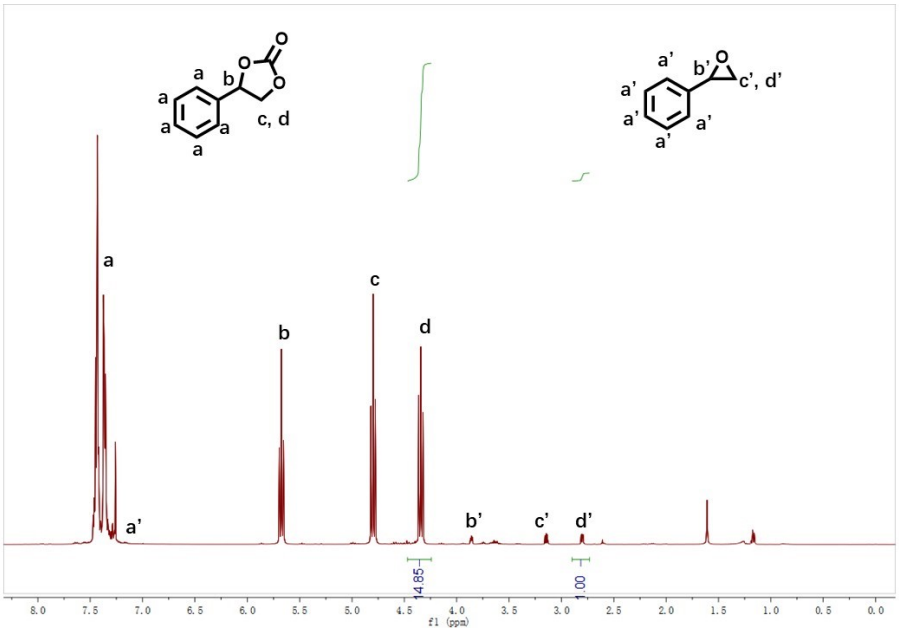

Fig. S28. ^{1}H NMR (400 MHz, CDCl3) spectrum of reaction mixture performed at 100 ℃ for 12 h with IrCu-I/GDY.

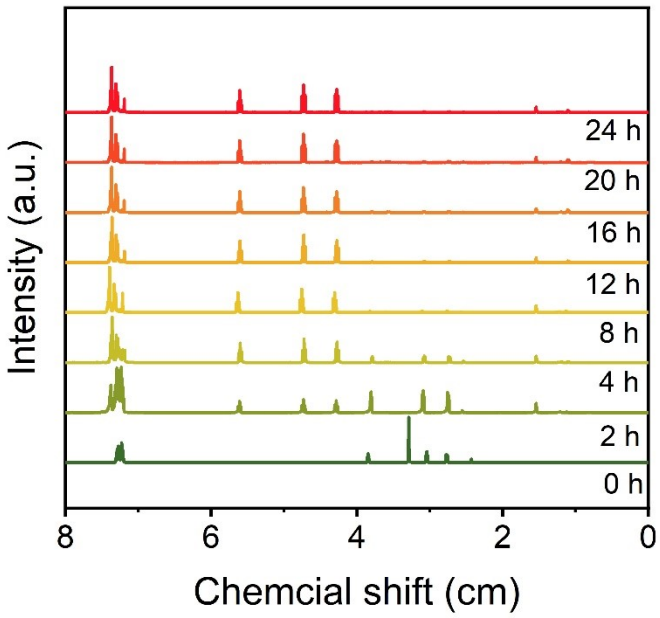

Fig. S29. Time course of the 1H NMR result of the catalytic product by IrCu-I/GDY performed at 100 ℃.

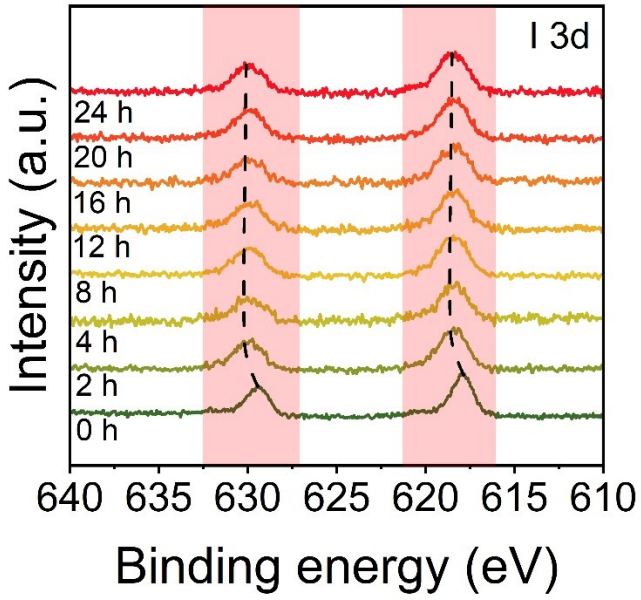

Fig. S30. I 3d spectra of IrCu-I/GDY during the catalytic processes.

Table S1. EXAFS fitting parameters at the Ir L edge for IrCu-Cl/GDY.

Shell	N[a]	R(Å)[b]	σ^2 (Å^2) [c]	ΔE_0 (eV)[d]	R factor
Ir-C1	2	2.27	0.00068	8.563	0.023
Ir-C2	3	2.08	0.00068	8.563	
Ir-Cl	1.4	2.34	0.00068	8.563	

[a] N: coordination numbers; [b] R: bond distance; [c] σ^2: Debye Waller factors; [d] ΔE_0: the inner potential correction; R factor: goodness of fit.

Table S2. EXAFS fitting parameters at the Cu K edge for IrCu-Cl/GDY.

Shell	N[a]	R(Å)[b]	σ^2 (Å^2) [c]	ΔE_0 (eV)[d]	R factor
Cu-C1	2.2	1.75	0.01368	4.853	0.012
Cu-C2	2.4	1.99	0.01368	4.853	
Cu-Cl	1.2	2.32	0.01368	4.853	

[a] N: coordination numbers; [b] R: bond distance; [c] σ^2: Debye Waller factors; [d] ΔE_0: the inner potential correction; R factor: goodness of fit.

Table S3. EXAFS fitting parameters at the Ir L edge for IrCu-I/GDY.

Shell	N[a]	R(Å)[b]	σ^2 (Å^2) [c]	ΔE_0 (eV)[d]	R factor
Ir-C1	1.7	2.00	0.00021	10	0.014
Ir-C2	8	2.16	0.00021	10	
Ir-I	1	2.71	0.00021	10	

[a] N: coordination numbers; [b] R: bond distance; [c] σ^2: Debye Waller factors; [d] ΔE_0: the inner potential correction; R factor: goodness of fit.

Table S4. EXAFS fitting parameters at the Cu K edge for IrCu-I/GDY.

Shell	N[a]	R(Å)[b]	σ^2 (Å^2) [c]	ΔE_0 (eV)[d]	R factor
Cu-C1	2	1.67	0.01001	10	0.0036
Cu-C2	2	2.06	0.01001	10	
Cu-I	0.5	2.76	0.01001	10	

[a] N: coordination numbers; [b] R: bond distance; [c] σ^2: Debye Waller factors; [d] ΔE_0: the inner potential correction; R factor: goodness of fit.

References

1 Kresse, G. & Hafner, J. Ab initio molecular dynamics for open-shell transition metals. Physical Review B - Condensed Matter 48, 13115-13118 (1993). https://doi.org:10.1103/physrevb.48.13115

2 Kresse, G. F. l., J. Efficient iterative schemes for ab initio total-energy calculations using a plane-wave basis set. Physical Review B - Condensed Matter 54, 169-185 (1996). https://doi.org:10.1103/PhysRevB.54.11169

3 John P. Perdew, K. B., and Matthias Ernzerhof. Generalized gradient approximation made simple. Phys. Rev. Lett 77 (1996).

4 Kohn, W. & Sham, L. J. Self-Consistent Equations Including Exchange and Correlation Effects. Physical Review 140, A1133-A1138 (1965). https://doi.org:10.1103/PhysRev.140.A1133

5 Grimme, S., Antony, J., Ehrlich, S. & Krieg, H. A consistent and accurate ab initio parametrization of density functional dispersion correction (DFT-D) for the 94 elements H-Pu. The Journal of chemical physics 132, 154104 (2010).

6 Wang, V., Xu, N., Liu, J.-C., Tang, G. & Geng, W.-T. VASPKIT: A user-friendly interface facilitating high-throughput computing and analysis using VASP code. Comput Phys Commun 267, 108033 (2021). https://doi.org:10.1016/j.cpc.2021.108033

7 Momma, K. & Izumi, F. VESTA: a three-dimensional visualization system for electronic and structural analysis. Journal of Applied Crystallography 41, 653-658 (2008). https://doi.org:10.1107/s0021889808012016